Environ. Sci. Technol. **2003**, *37,* 1905−1911

Dissolved Oxygen Imaging in a Porous Medium to Investigate Biodegradation in a Plume with Limited Electron Acceptor Supply

WEI E. HUANG,*,† SASCHA E. OSWALD,† DAVID N. LERNER,† COLIN C. SMITH,† AND CHUNMIAO ZHENG‡

Groundwater Protection and Restoration Group, Department of Civil and Structural Engineering, University of Sheffield, United Kingdom, and Department of Geological Sciences, University of Alabama, Tuscaloosa, Alabama

A novel combination of noninvasive imaging with an oxygen sensitive fluorescent indicator was developed to investigate the biodegradation processes occurring at the fringe of a solute plume, where the supply of oxygen was limited. A thin transparent porous matrix (156 × 120 × 3 mm) was made from quartz plates and quartz sand (212−300 μm) and enriched with acetate-degrading bacteria. A degrading plume developed from a continuous acetate source in the uniform flow field containing dissolved oxygen. Ruthenium (Π)-dichlorotris(1,10-phenanthroline) ($Ru(phen)_3Cl_2$), a water-soluble fluorescent dye, was used as an indicator of dissolved oxygen. The fluorescence intensity was dependent on the concentration of oxygen because the dissolved oxygen acted as collisional quencher. The oxygen distribution was interpreted from images recorded by a CCD camera. These two-dimensional experimental results showed quantitatively how the oxygen concentrations decreased strongly at the narrow plume fringe and that oxygen was depleted at the core of the plume. Separately, dispersivity was measured in a series of nonreactive transport experiments, and biodegradation parameters were evaluated by batch experiments. Two-dimensional numerical simulations with MT3D/RT3D used these parameters, and the predicted oxygen distributions were compared with the experimental results. This measurement method provides a novel approach to investigate details of solute transport and biodegradation in porous media.

Introduction

Contamination of groundwater by organic chemicals is a widespread environmental problem. Because of the potentially high costs of remediation, the scientific prediction of natural attenuation processes is of great practical importance. For pollutants degraded by biological oxidation, natural attenuation is usually limited by the supply of electron acceptors (*1*, *2*). In many cases, the electron donor load of the plume is substantial, while the availability of electron acceptors (e.g., O_2, NO_3^-) is limited. Biodegradation is often concentrated at the fringe of the plume and significantly controlled by transverse dispersion processes (*3*). Electron acceptors are replenished by transverse mixing, and the toxicity of contaminants is reduced by dilution processes arising from transverse dispersion. Therefore, the rate of biodegradation in a stable plume of reduced compounds can depend to a large extent on the mixing processes at the fringe. Information on contaminant mixing processes in the subsurface becomes crucial in order to predict natural attenuation.

Obtaining well-defined and spatially comprehensive data from field tests is very difficult, so well-controlled laboratory models are attractive for investigating fundamental processes and for validating numerical models. The transverse mixing zone at the fringe can be very thin, and sampling in this thin zone is very difficult and will inevitably disturb the plume. Measurements based on a noninvasive imaging technique are therefore advantageous. Huang et al. (*4*) described a noninvasive imaging technique measuring fluorescent dye tracers and demonstrated its ability to accurately simulate transverse dispersion processes with a conservative tracer. Here we extend this methodology to the more complex process of biodegradation within a plume.

Oxygen quenched luminescence sensors have been widely used to measure oxygen concentrations (*5*−*10*). Some oxygen sensors are based on fluorescence from pyrene derivatives (*11*−*13*). However, the solubility of pyrene derivatives in the water is low and the intensity of the fluorescence is too weak to be efficiently detected by common CCD cameras. In comparison, the ruthenium complex is particularly attractive for detecting dissolved oxygen in the water because it has a high luminescent quantum yield, large Stokes shift, and strong absorption in the blue−green spectral region, and more importantly, it is water soluble (*14*−*17*). Under UV light, the fluorescent intensity of the ruthenium complex is a function of the concentration of oxygen (*15*). By combining our imaging technique with this fluorescent indicator, the mixing and consumption of oxygen in the plume can be directly measured without any disturbance.

Our goal is to deepen the understanding of biological oxidation in porous media and improve our confidence in field applications of natural attenuation. Thus, the principal aim of this paper is to report a novel approach to the observation and quantification of coupled transport and biodegradation processes in the laboratory. The secondary aim is to compare these with several conceptual models through numerical simulation. We illustrate these through the scenario of a plume with substantial electron donor load in groundwater containing limited electron acceptors.

Conceptual and Mathematical Representations of Solute Transport and Biodegradation

Solute Transport. Solute transport in a three-dimensional flow field can be described by

$$\frac{\partial C}{\partial t} = -\frac{\partial}{\partial x_i}(v_i C) + \frac{\partial}{\partial x_i}\left(D_{ij}\frac{\partial C}{\partial x_j}\right) + \sum_{k=1}^{m} R_k \quad i, j = 1,2,3 \quad (1)$$

where C = solute concentration, v_i = pore water velocity component in the x_i direction, t = time, D_{ij} = components of the dispersion coefficient tensor, x_i, x_j = Cartesian coordinates, and $\Sigma_{k=1}^{m} R_k$ is a chemical/biological reaction term in which R_k is the rate for reaction k and m is total number of chemical reactions of this solute.

* Corresponding author phone: ++44 1970 622339; fax: ++44 1970 622350; e-mail: wwh@aber.ac.uk. Now located at Institute of Biological Sciences, University of Wales Aberystwyth, Ceredigion, SY2 3DA, U.K.

† University of Sheffield.

‡ University of Alabama.

10.1021/es020128b CCC: $25.00
Published on Web 03/27/2003

Domenico and Robbins (*18*) provided 2-dimensional analytical solutions to eq 1 for conservative transport in a uniform flow field. Where solute is continuously injected at a constant line source, equations (2) and (3) give these solutions for steady state and transient conditions.

$$C(x,y) = (C_0/2)\left\{erf\left[\frac{(y + Y/2)}{2(D_T x/v)^{1/2}}\right] - erf\left[\frac{(y - Y/2)}{2(D_T x/v)^{1/2}}\right]\right\} \quad (2)$$

$$C(x,y,t) = (C_0/4)erfc\left[\frac{(x - vt)}{2(D_L t)^{1/2}}\right]\left\{erf\left[\frac{(y + Y/2)}{2(D_T x/v)^{1/2}}\right] - erf\left[\frac{(y + Y/2)}{2(D_T x/v)^{1/2}}\right]\right\} \quad (3)$$

$$D_L = a_L v + D^* \quad (4)$$

$$D_T = a_T v + D^* \quad (5)$$

Where for clarity we adopt x and y for the Cartesian coordinates (previously defined as x_1 and x_2 in eq 1), C = solute concentration, C_0 = source concentration, Y = length of the source in the y direction (centered at the origin), D_L and D_T = longitudinal and transverse dispersion coefficients, a_L and a_T = longitudinal and transverse dispersivities, D^* = the effective molecular diffusion coefficient, and v = the pore water velocity which is in the x direction.

Biodegradation. Respiration is an important biodegradation process in which microbes employ electron acceptors when they degrade organic compounds. Two widely used conceptual and mathematical models for aerobic degradation are the instantaneous reaction and the double Monod model.

In the case of instantaneous reaction, the following algorithm models the removal rates in numerical simulations (*19*).

$$S(t + 1) = S(t) - O(t)/F, \text{ and } O(t + 1) = 0, \text{ when } S(t) > O(t)/F \quad (6)$$

$$O(t + 1) = O(t) - S(t)F, \text{ and } S(t + 1) = 0, \text{ when } O(t) > S(t)F \quad (7)$$

where F is the stoichiometric ratio of oxygen to substrate consumed, and $S(t)$, $S(t + 1)$, $O(t)$, and $O(t + 1)$ are substrate and oxygen concentrations at times t and $t + 1$.

The double Monod model can also describe aerobic degradation. This gives the reaction rate term R_k in eq 1 as

$$\frac{dS}{dt} = -M \times \frac{\mu_m}{Y_{x/c}} \times \frac{S}{K_s + S} \times \frac{O}{K_o + O} \quad (8)$$

$$\frac{dO}{dt} = -M \times \frac{\mu_m}{Y_{x/o}} \times \frac{S}{K_s + S} = -M \times F \times \frac{\mu_m}{Y_{x/c}} \times \frac{S}{K_s + S} \times \frac{O}{K_o + O} \quad (9)$$

where M = the total microbial concentration (dry biomass/fluid volume), and is assumed to be constant for all transport simulations in this paper, μ_m = maximum specific growth rate, $Y_{x/c}$ = growth yield for substrate as carbon source (dry biomass/mass carbon source consumed), $Y_{x/o}$ = growth yield for oxygen (dry biomass/mass oxygen consumed), K_s = the half-saturation constant for the substrate and K_o = the half-saturation constant for oxygen (*19, 20*).

These equations may be solved numerically by programs such as MT3D and RT3D (*21, 22*). In this paper, the analytical solutions (2) and (3) and MT3D were used to simulate conservative solute transport and evaluate physical parameters. RT3D, and in one case MT3D, with a total variation diminishing (TVD) scheme, were used to simulate reactive transport and to obtain the resulting oxygen distribution. Peclet and Courant criteria (e.g., (*23*)) were satisfied by the choice of grid cell and time step size.

Experimental Materials

The primary experiments involve nonreactive and reactive transport in a transparent quasi 2-D porous matrix. The distributions of relevant species were ascertained through the imaging of fluorescent tracers.

Nonreactive Transport Experiment. The basic experimental equipment has been previously described (*4*) and modifications and additional materials are as follows; all chemicals were supplied by Sigma-Aldrich.

Porous Matrix. For the experiments the porous medium was made of high quality quartz sand (212−300 μm) in preference to ordinary glass because it transmits UV with little loss. The quartz sand was packed into a quartz box of internal dimensions 156 × 120 × 3 mm to form a micromatrix. The thinness of the box relative to its width and length means that it is effectively a 2-dimensional matrix. Each end of the matrix terminates in a chamber, separated from the matrix. The matrix box was partially filled with water, and then the quartz sand/water mixture was slowly poured into the box. At the same time, the emplaced beads were stirred to release gas bubbles. The average porosity n of the matrix was determined (n = 0.49) from the mass of quartz sand.

Source. The plume was injected by a syringe pump (Harvard apparatus, model 2400003) into the porous matrix through an 8-mm i.d. pipe, which ran through the thickness of the model and was perforated in the flow direction.

CCD Camera. The process of mass transport was recorded by a Hitachi color KP-D581 CCD camera. The resolution of the camera was 811(H) × 508(V) pixels and the minimum object illumination was 0.02 lux. An UV filter was installed in the front of the camera to block stray UV light. The distance between the CCD camera and the box was 596 mm.

Reactive Transport Experiment. Enhancements to the nonreactive transport setup were as follows.

Fluorescent Oxygen Indicator. $Ru(phen)_3Cl_2$, that is ruthenium(II)-dichlorotris(1,10-phenanthroline), was used at a concentration of 1.0×10^{-4} M.

Under UV (450 nm) light, $Ru(phen)_3^{2+}$ in the quartz sand matrix can be excited and emits fluorescent light at 590−600 nm (*16*). If a dye loses its excitation energy by dissipation after a collision with another molecule and thus returns to the ground state without emission of fluorescent light, this is referred to as quenching (*24*). Oxygen is a good quencher for $Ru(phen)_3^{2+}$, and furthermore, the regeneration of fluorescence of $Ru(phen)_3^{2+}$ is prompt (*7, 10*). Therefore, the more oxygen present in solution, the lower the fluorescent intensity of $Ru(phen)_3^{2+}$. This allows an in-situ and online evaluation of oxygen concentration by measuring intensity of $Ru(phen)_3^{2+}$ through a CCD camera. The quenching effect is a function of temperature and oxygen concentration. At constant temperature, the luminescent intensity of $Ru(phen)_3^{2+}$ is a direct indicator of the oxygen concentration (*24*). Oxygen-free water shows the strongest fluorescence intensity I_0. With increasing oxygen concentration the light intensity decreases linearly as described by the Stern−Volmer equation (*16, 25*)

$$\frac{I_0}{I} = 1 + K_{SV}O \quad (10)$$

where I = the luminescence intensity in the presence of quencher (O_2) and K_{SV} = the Stern−Volmer constant.

Mineral Medium. The mineral medium consisted of 0.1% Na_2HPO_4, 0.1% KH_2PO_4, 0.1% NH_4Cl, 0.05% $MgSO_4$, 0.00712%

TABLE 1. Water and Tracer Flow Rates Used in the Non-Reactive Experiments

water flow rate (mL/min)	injection rate of sodium fluorescein (μL/min)	water velocity (m/s)
0.13	8.6	1.25×10^{-5}
0.27	18.0	2.50×10^{-5}
0.40	26.7	3.75×10^{-5}
0.94	62.7	8.67×10^{-5}
1.48	98.7	1.37×10^{-4}
2.04	136.0	1.89×10^{-4}

$Ru(phen)_3Cl_2$ (1.0×10^{-4} M), and 5−8 drops of saturated $CaCl_2$ and $FeSO_4$ solutions per 1000 mL of ultrahigh-quality water.

Carbon Source. The carbon source was potassium acetate (KAc).

Microbe Culture on Quartz Matrix. Bacteria were isolated from a field soil and enriched in the mineral medium and 1000 mg/L Ac. The solute transport experiments required a microbe population to be present on the matrix. This was achieved by mixing the quartz sand with the mineral medium and packing it in a glass column as previously described (*26*). The bacteria and Ac (as the sole carbon source) were continuously introduced into the column while oxygen was bubbling from the column base. After 24 h, the supply of Ac was cut off. Samples of liquid were then taken at regular intervals until the concentration of Ac (measured by ion chromatograph) decreased to zero. At this stage the quartz sand was ready to be incorporated into the solute transport experiment without introducing additional unwanted Ac. Because the bacteria were in the stationary phase after enrichment in this experiment, we have assumed that the population was approximately in a steady state between growth and decay. A sample of the sand was used to estimate biomass by vigorous stirring to release cells from the surfaces.

Experimental Procedures

Nonreactive transport experiments and batch experiments were conducted to determine the model transport parameters (D^*, a_L, a_T) and biological parameters (μ_m, K_o, K_s, F, *and* $Y_{x/c}$). Reactive transport experiments were then conducted to investigate the oxygen distribution and biodegradation processes in the porous medium. All experiments were undertaken at 16 °C.

Nonreactive Solute Transport Parameters. *Experimental Procedures.* The experimental setup has been described previously (*4*). The porous matrix had a water flow induced by a pump at the downstream end. A tracer, 8 mg/L sodium fluorescein, was introduced into the porous matrix through the perforated pipe by a syringe pump generating the same flux as the general water flow alongside the pipe (Table 1). The fluorescent tracer was illuminated by UV light (located 176 mm behind the porous matrix), observed by a CCD camera, and the images were captured and analyzed. Calibration was performed by passing different concentrations of sodium fluorescein through the whole matrix and processing the resulting images.

Biodegradation Parameters. *Analytical Techniques.* Cell suspensions were monitored by spectrometry (UV500, Unicam) at 600 nm (1 OD600 unit = 0.32 g dry biomass/L). The measurement was calibrated by harvesting cells by centrifugation at 4000 rpm for 15 min, and the biomass was then determined gravimetrically after drying at 105 °C. Concentrations of Ac were analyzed by ion chromatography (Dionex DX-120). Dissolved oxygen was monitored by an oxygen probe (OX20 portable oxygen meter, Walden).

Batch Growth Kinetics. Batch experiments were undertaken to investigate the relationship between oxygen consumption and acetate concentration during biodegradation. The bacteria, 500 mL of mineral medium, fluorescent indicator (1.0×10^{-4} M), and Ac (100 mg/L) were mixed by magnetic stirrer (Hanna, HI-300N) in a sealed 500-mL brown bottle. Dissolved oxygen was continuously monitored in the batch reactor by the oxygen probe. Every 20 min 5-mL samples were taken out of the bottle; a syringe was filled with pure nitrogen, injected into the bottle, and then the same volume of liquid sample taken. This prevented additional oxygen from entering the system. Subsamples (2 mL) were used to measure the concentration of bacteria by spectrometry at 600 nm. The remaining 3 mL were filtered by 0.2-μm membranes and divided. A 2-mL subsample of the filtered samples was put into a cuvette, purged with nitrogen gas for 10 min to remove oxygen, and used to measure $Ru(phen)_3^{2+}$ by the absorbance at 420 nm (*15*). The last 1 mL of the filtered samples was diluted 10× for acetate determination.

Half Saturation Constants of Acetate and Oxygen. Two sets of batch experiments were conducted to determine K_o and K_s according to a method (*36*, *38*). When the Ac concentration, and thus the carbon source level, is high, dissolved oxygen is the single nutrient limiting growth. Assuming Monod kinetics, the specific growth rate μ of M can be written as

$$\mu = \mu_m \frac{O}{K_o + O} \tag{11}$$

A range of dissolved oxygen concentrations was created by continuously pumping a mixture of air and nitrogen into the batch reactor while μ was measured assuming an exponential growth of biomass M.

In the second set of experiments the conditions were inverted and acetate was the limiting nutrient. The initial growth rate was measured for a range of initial concentrations of Ac while continuously pumping excess oxygen into the batch reactor. By measuring the biodegradation close to the start of the reaction, changes of Ac are negligible and thus Ac concentration can be regarded as constant.

Nonlinear regression software (SigmaPlot, Ver7.1, SPSS Inc.) was used to determine maximum specific growth rate (μ_m) and half saturation constants K_o and K_s by fitting the experimental data of the specific growth rate.

Reactive Transport. Bacteria were cultured on quartz sand as described above and packed in the aquifer box ready for the reactive transport experiments. The procedures were similar to those of the nonreactive experiments. Water with 6.64 mg/L dissolved oxygen, carbon-free mineral nutrient, and $Ru(phen)_3Cl_2$ was pumped uniformly through the porous matrix at a water velocity of 1.25×10^{-5} m/s. Ac solution (1000 mg/L) with 6.64 mg/L dissolved oxygen and $Ru(phen)_3Cl_2$ was then introduced into the source pipe at a flux of 8.6 μL/min. Ac was the sole carbon source for the biodegradation. Bacteria had been cultured on the surface of the quartz sands, and these bacteria degraded the acetate while consuming oxygen. UV light was used to excite the $Ru(phen)_3^{2+}$ which was uniformly distributed in the porous matrix. As in the nonreactive experiment, the images were recorded by a CCD camera and then processed by computer.

Results and Discussion

Nonreactive Transport. *Derivation of Transport Parameters.* The experimental results were matched to eqs 2 and 3 to obtain the transverse and longitudinal dispersion coefficients. Values were obtained by minimizing the total relative error and analyzing model efficiency (*4*). Figure 1 illustrates a typical match between model and data for steady-state

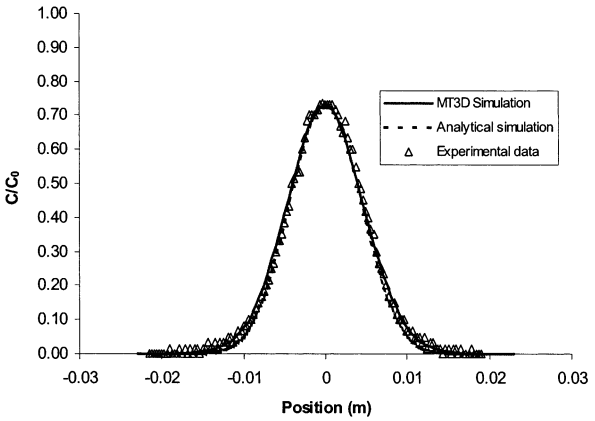

FIGURE 1. Observed and calculated fluorescein concentrations for a section across a conservative plume 98 mm downgradient of the source at steady state (pore water velocity 1.25 × 10^{-5} m/s)

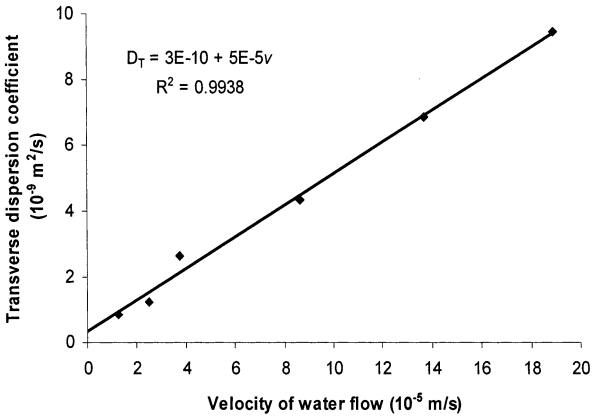

FIGURE 2. Relation between the transverse dispersion coefficient (D_T) and pore water velocity (v) for fluorescein.

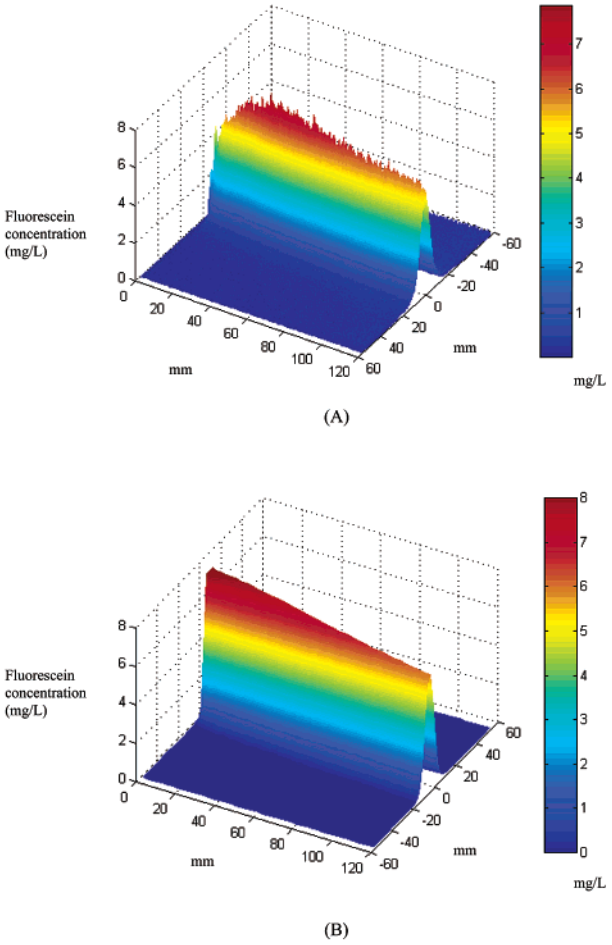

FIGURE 3. Comparison of (A) experimental data of fluorescein distribution and (B) MT3D simulation, in steady state.

conditions at a transverse section 98 mm downstream of the source. The transverse dispersion coefficient is 8.5 × 10^{-10} m^2/s.

Transverse dispersion coefficients were obtained for several water velocities (Figure 2). There is a linear relation conforming to eq 5, with a transverse dispersivity a_T of 5.0 × 10^{-5} m and an effective molecular diffusion coefficient of $D^* = 3.0 \times 10^{-10}$ m^2/s ($R^2 = 0.9938$). For comparison, the diffusion coefficient in free solution (between 5.0 × 10^{-10} (*27*) and 5.7 × 10^{-10} m^2/s (*28*)) can be used with an empirical equation (*29*) and temperature can be corrected to estimate the effective diffusion coefficient to be 1.7−2.9 × 10^{-10} m^2/s. The experimentally derived value is in good agreement with these values within the likely errors in its determination.

The steady state distribution of a conservative tracer is independent of longitudinal dispersion. However, to numerically simulate the biodegrading plume, longitudinal dispersivity is needed as an additional input parameter. Longitudinal dispersivity α_L was derived from the transient fluorescein distribution along the center line of the plume. Values in the range $\alpha_L = 0.5 - 1.0$ mm gave a reasonable fit to the measured data and thus $\alpha_L = 0.75$ mm was taken as a representative value. Only data for $x > 20$ mm were used for this analysis because the shadow of the injection pipe artificially lowered the measured light intensity close to the source.

MT3D simulations were based on the longitudinal and transverse dispersivities determined above ($\alpha_T = 0.05$ mm and $\alpha_L = 0.75$ mm). Figure 3 shows for the steady state a very good agreement between the experimental fluorescein distribution and the MT3D simulation. A comparison of measured concentrations along the center line, analytical and MT3D solutions for a line source, and MT3D simulations for a source shaped like the actual pipe showed a good agreement within the uncertainty of the measurement. For modeling of the reactive transport a source shaped like the actual pipe was used.

Table 2 compares the longitudinal and transverse dispersivities from this study with results reported in the literature. Those experiments were conducted at similar velocities and in similar porous media and confirm the results of this study.

Biodegradation Parameters. In the batch experiments, both the acetate and oxygen concentrations decreased with time showing that both are consumed by a degradation reaction (Figure 4). There are no other electron donors or electron acceptors present in significant quantities, therefore it can be assumed that the bacteria degraded acetate by consuming oxygen. Full oxidization of Ac coupled to reduction of oxygen is described by

$$CH_3COO^- + 2O_2 + H^+ \rightarrow 2CO_2 + 2H_2O \qquad (12)$$

In this eq 12 the stoichiometric ratio, F, is 1.08 mg O_2/mg Ac. A regression of the oxygen and Ac consumption data from the batch experiments in Figure 4 showed that they have a linear relationship with a stoichiometric ratio, F, of 0.39 mg O_2/mg Ac ($R^2 = 0.9639$). This linear relationship strongly supports the assumption that the decrease of oxygen results only from degradation of Ac and that oxygen is the only electron acceptor for Ac degradation. However, the lower measured F implies that not all Ac was oxidized to CO_2 and

TABLE 2. Results of This Study Compared with Other Laboratory Results

material	pore water velocity (m/s × 10^{-5})	grain size (m × 10^{-6})	porosity	longitudinal dispersivity (m × 10^{-3})	transverse dispersivity (m × 10^{-3})	reference
quartz glass beads & plates	1.25−18.90	212−300	0.49	0.5−1.0	0.05	this study
glass beads	0.57	60−100	0.38		0.04	(*4*)
glass beads	25	570	0.28	0.5		(*40*)
glass beads	7.56−7.94 8.64−9.52	480	0.39	0.17−0.38	0.009−0.044	(*41*)
beads	3.85−8.80	163−595	0.34	0.88		(*42*)
glass beads	0.8	250	0.4		0.01−0.4	(*43*)
plastic spheres	11.6−130	960	0.36	0.6	0.034	(*44*)

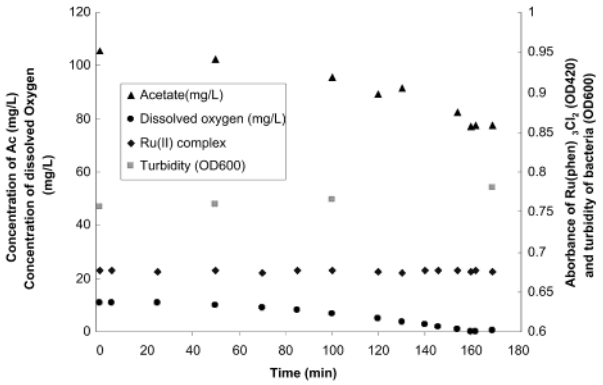

FIGURE 4. Batch experimental results showing changes with time of Ac and oxygen (left axis), and $Ru(phen)_3Cl_2$ and biomass (right axis).

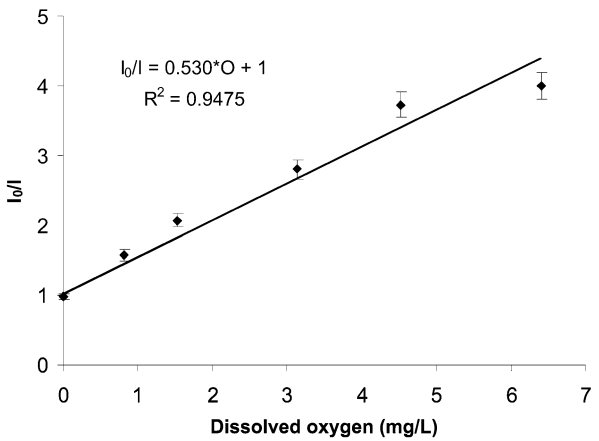

FIGURE 5. Calibration of relative intensity (I_0/I) against dissolved oxygen concentration in the porous medium.

H_2O, and some Ac was used to produce cell mass. The biomass yield $Y_{x/c}$ was measured to be 0.32 g of dry mass per gram of Ac. The use of empirical formula, derived from wastewater treatment plants, to estimate $Y_{x/c}$ from F would give somewhat larger values for $Y_{x/c}$.

$Ru(phen)_3^{2+}$ is a polycyclic aromatic hydrocarbon and it is expected to be recalcitrant to degradation by common bacteria. Figure 4 shows that $Ru(phen)_3^{2+}$ remained unchanged during the Ac biodegradation, and can be assumed conservative.

The experimental data were fitted using a Monod relationship with a maximum specific growth rate μ_m of 0.005 min^{-1}, K_o of 0.01 mg/L, and K_s of 2.1 mg/L (data fit not shown). These values of K_o and K_s are within the wide range reported of 0.0004−0.45 mg/L (*30*−*37*) and 0.19−14.0 mg/L (*36, 38*), respectively. The fitted value of μ_m was consistent between the two experiments.

The variables μ_m, K_o, K_s, F, and $Y_{x/c}$ reflect the intrinsic physiological properties of a particular type of microorganism (*39*). As the same culture was used in the transport experiments, these batch parameters were used for the initial simulation of the transport and degradation experiment.

Oxygen Calibration. Different concentrations of dissolved oxygen within the mineral medium (including $Ru(phen)_3Cl_2$ at 1.0×10^{-4} M) were passed through the whole matrix and imaged as described above. The fluorescence intensity was used to calibrate the indicator as a measure of oxygen concentration. The data follow the linear Stern−Volmer equation closely as observed by others (*16, 25*) with K_{sv} = 0.53 L mg^{-1} (Figure 5).

Reactive Transport. Figure 6 shows the experimental result of oxygen distributions in the porous medium at two times. After 672 min (Figure 6A), the plume had not yet reached steady state. In the core of the plume the oxygen was nearly exhausted. Oxygen can also be observed to mix with Ac at the front of the plume, but this mixing zone is small compared with the long lateral fringe and larger area of transverse mixing. This suggests that transverse mixing will be responsible for most of the aerobic degradation in

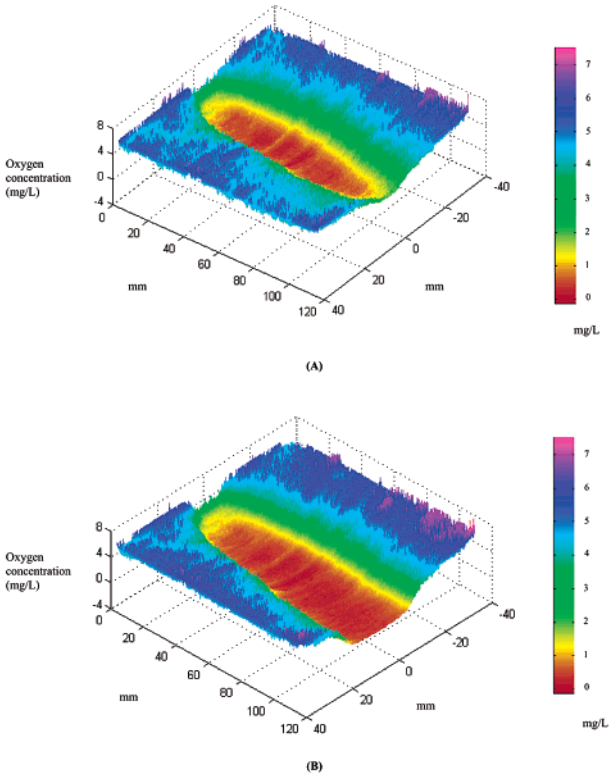

FIGURE 6. Experimental oxygen distributions in the porous medium: (A) t = 672 min, unsteady state; (B) t > 1440 min, steady state.

long transient plumes, and for all the degradation in a steady-state plume.

After 1440 min (Figure 6B), the plume had definitely reached a steady state. The core of the plume was an oxygen depleted zone with negligible aerobic degradation. However,

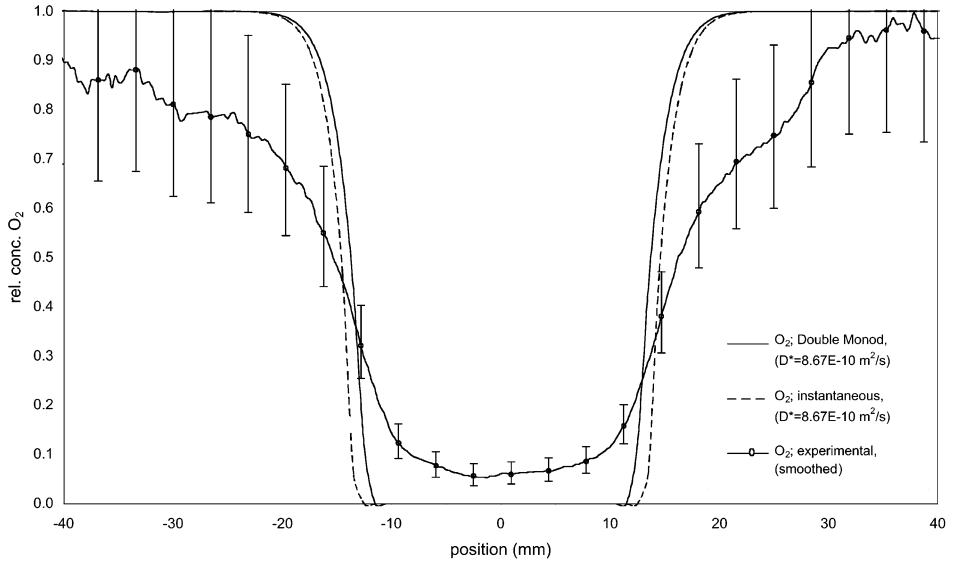

(A)

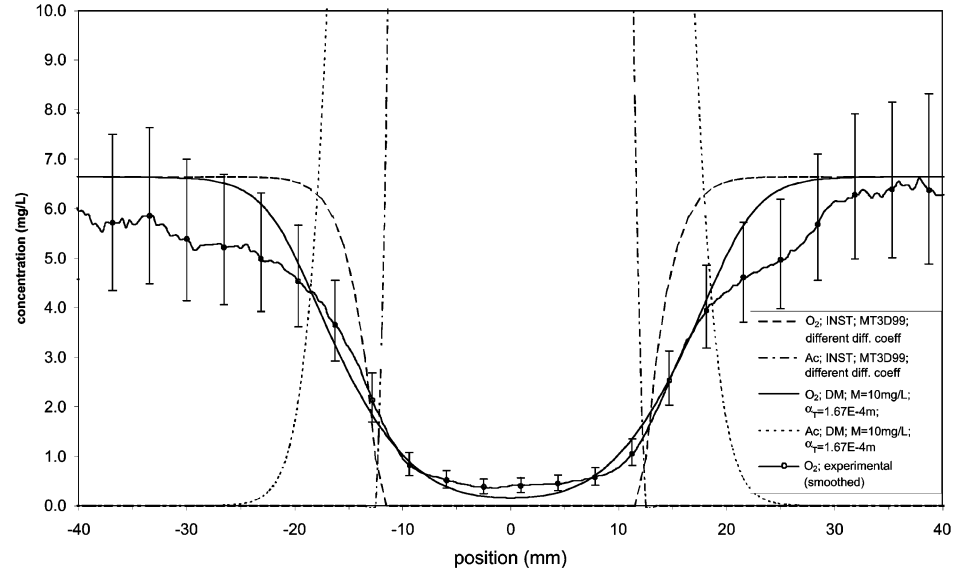

(B)

FIGURE 7. Comparison of different reaction models with experimental results at section $x = 76$ mm. (A) Double Monod and instantaneous models (normalized). (B) Instantaneous model with different diffusion coefficients D^*, and double Monod model with adapted value of $M^*\mu_m/Y_{x/c}$ and dispersivity (original data). Error bars are not shown for all data and become larger at large oxygen concentrations due to the reciprocal nature of the Stern−Volmer equation.

at the fringe, oxygen is mixed into the plume by transverse dispersion and consumed by biodegradation.

Numerical Simulation of Reactive Transport. Instantaneous and double Monod reaction models were employed to simulate the experimental results. Almost all physical and biological parameters have been evaluated by the nonreactive transport and batch experiments as described above. The original numerical codes used a single diffusion coefficient for all species, and an average value of 8.7×10^{-10} m^2/s was used. Initially, no parameter was fitted for the simulations and Table 3 gives the parameter values.

Figure 7A shows that instantaneous and double Monod models predicted very similar concentration profiles, indicating that the reaction rates in the batch experiments had been fast. Both models were able to predict the depletion of oxygen at the core of the plume, but did not exactly fit the observed change in oxygen concentration at the plume fringe. Both models predict closely the position of the plume fringe, defined as oxygen having half the maximum concentration value. The concentration profiles of the models are too sharp, whereas the experimental data showed that active biodegradation took place in a broader area, at least at this laboratory scale.

Two hypotheses were tested to explain the lack of fit: first, that the difference in diffusion coefficients between Ac and oxygen was significant, and, second, that the parameters values from batch and nonreactive experiments did not transfer directly to the reactive transport case. An upgraded version of MT3D99 (*22*) was used to simulate the instantaneous model with different diffusion coefficients. Figure 7B shows that the result is a less steep oxygen concentration gradient, but the change is not enough to fit the measured data much better.

Three of the Monod parameters (M, μ_m, and $Y_{x/c}$) appear in eqs 8 and 9 as a product. They all have some uncertainty of measurement, and biodegradation behavior may be

TABLE 3. Values of Transport and Biodegradation Parameters Including Those Used for the Reactive Simulations

parameter	value
physical model size (mm)	120 × 156 × 3
typical grid resolution D_x, D_y (mm)	1 × 1
layer thickness (mm)	3
porosity	0.49
longitudinal dispersivity (m)	7.5×10^{-4}
transverse dispersivity (m)	5×10^{-5}
effective pore diffusion coefficient for Ac (m^2/s)[a]	5.3×10^{-10}
effective pore diffusion coefficient for O_2 (m^2/s)[a]	1.2×10^{-9}
pore water velocity (m/s)	1.25×10^{-5}
equivalent carbon source size (mm)	8
acetate concentration (mg/L)	1000
oxygen concentration (mg/L)	6.64
maximum specific growth rate μ_m (min^{-1})	0.005
ratio of O_2/Ac, F	0.39
growth yield $Y_{x/c}$ (g dry cells/g Ac)	0.32
growth yield $Y_{x/o}$ (g dry cells/g O_2)[b]	0.82
microbial concentration (mg/L)	120
half saturation constant for oxygen K_o (mg/L)	0.01
half saturation constant for acetate K_s (mg/L)	2.1
initial estimate of product $M^*\mu_m/Y_{x/c}$ (mg/L min^{-1})	1.875
final value of product $M^*\mu_m/Y_{x/c}$ (mg/L min^{-1})	0.156

[a] Calculated from literature values for diffusion in free solution based on the tortuosity factor determined in the nonreactive experiments. [b] Dependent parameter, shown for comparison only.

different in the unstirred medium of the experiment. In addition, the dispersivity may be larger than that measured in the nonreactive experiment. After some sensitivity analysis, a simulation with dispersivity values increased by a factor of about 3 and the product $M^*\mu_m/Y_{x/c}$ decreased by a factor of 12 (performed via a change of M only) fits the experimental data very well (Figure 7B). The increase in dispersion would imply that there was partial blocking of pores by biomass, which would increase tortuosity and dispersivity. The decrease of $M^*\mu_m/Y_{x/c}$ would imply that the active and attached biomass was lower than estimated, and/or that $Y_{x/c}$ was larger than measured.

The double Monod reaction model is able to reproduce the observed results best, because it allows electron acceptors and the carbon source to be present at the same location which is the more appropriate model of the two. The modeling results show that the location of the plume fringe is principally controlled by transverse dispersion, while the gradients of Ac and oxygen are also controlled by the biodegradation parameters.

The comparison with the numerical simulation shows how important it is to collect experimental data with high resolution to understand biodegradation processes. The new imaging technique for oxygen provides such data. However, it was difficult to obtain independent batch estimates of biodegradation parameters, which were valid for the conditions of the experiment with biodegradation and transport acting at the same time. Therefore, there is scope for further experimental research to understand why biodegradation in the batch and flow systems behave differently.

Acknowledgments

We appreciate the helpful suggestions for the experiments given by Professor Bob Watkinson, and the help of Ian Watson to confirm the modeling results, both at GPRG. This research was sponsored by the U.K. Environment Agency and an ORS award from Universities U.K.

Literature Cited

(1) Oya, S.; Valocchi, A. J. *Water Resour. Res.* **1998**, *34*, 3323−3334.
(2) Cirpka, O. A.; Frind, E. O.; Helmig, R. *J. Contam. Hydrol.* **1999**, *40*, 159−182.
(3) Lerner, D. N.; Thornton, S. F.; Spence, M. J.; Banwart, S. A.; Bottrell, S. H.; Higgo, J. J.; Mallinson, H. E. H.; Pickup, R. W.; Williams, G. M. *Ground Water* **2000**, *38*, 922−928.
(4) Huang, W. E.; Smith, C. C.; Lerner, D. N.; Thornton, S. F.; Oram, A. *Water Res.* **2001**, *36*, 1843−1853.
(5) Lee, M.; Schladow, S. G. *Water Res.h* **2000**, *34*, 2842−2845.
(6) Watkins, A. N.; Wenner, B. R.; Jordan, J. D.; Xu, W. Y.; Demas, J. N.; Bright, F. V. *Appl. Spectrosc.* **1998**, *52*, 750−754.
(7) Klimant, I.; Kuhl, M.; Glud, R. N.; Holst, G. *Sens. Actuators, B* **1997**, *38*, 29−37.
(8) Holst, G.; Glud, R. N.; Kuhl, M.; Klimant, I. *Sens. Actuators, B* **1997**, *38*, 122−129.
(9) Holst, G.; Kohls, O.; Klimant, I.; Konig, B.; Kuhl, M.; Richter, T. *Sens. Actuators, B* **1998**, *51*, 163−170.
(10) Rosenzweig, Z.; Kopelman, R. *Sens. Actuators, B* **1996**, *36*, 475−483.
(11) Wolff, L. M.; Hanratty, T. J. *Exp. Fluids* **1994**, *16*, 385−392.
(12) Vaughan, W. M.; Weber, G. *Biochemistry* **1970**, *9*, 464−473.
(13) Lee, E. D.; Werner, T. C.; Seitz, W. R. *Anal. Chem.* **1987**, *59*, 279−283.
(14) Amao, Y.; Okura, I. *Polym. J.* **2000**, *32*, 452−455.
(15) Carraway, E. R.; Demas, J. N.; Degraff, B. A.; Bacon, J. R. *Anal. Chem.* **1991**, *63*, 337−342.
(16) Garcia-Fresnadillo, D.; Marazuela, M. D.; Moreno-Bondi, M. C.; Orellana, G. *Langmuir* **1999**, *15*, 6451−6459.
(17) Li, L.; Walt, D. R. *Anal. Chem.* **1995**, *67*, 3746−3752.
(18) Domenico, P. A.; Robbins, G. A. *Ground Water* **1985**, *23*, 476−485.
(19) Borden, R. C.; Bedient, P. B. *Water Resour. Res.* **1986**, *22*, 1973−1982.
(20) Molz, F. J.; Widdowson, M. A.; Benefield, L. D. *Water Resour. Res.* **1986**, *22*, 1207−1216.
(21) Clement, T. P. *RT3D − A Modular Computer Code for Simulating Reactive Multi-Species Transport in 3-Dimensional Groundwater Aquifers*; PNNL-11720, Pacific Northwest National Laboratory: Richland, WA, 1997.
(22) Zheng, C. M.; Bennett, G. D. *Applied Contaminant Transport Modeling, Second Ed.*; John Wiley & Sons: New York, 2002.
(23) Daus, A. D.; Frind, E. O.; Sudicky, E. A. *Adv. Water Resour.* **1985**, *8*, 86−95.
(24) Slavik, J. *Fluorescent Probes in Cellular and Molecular Biology*; CRC Press: Boca Raton, FL, 1994.
(25) McEvoy, A. K.; McDonagh, C. M.; MacCraith, B. D. *Analyst* **1996**, *121*, 785−788.
(26) Li, G.; Huang, W.; Lerner, D. N.; Zhang, X. *Water Res.* **2000**, *34*, 3845−3853.
(27) Radomsky, M. L.; Whaley, K. J.; Cone, R. A.; Saltzman, W. M. *Biomaterials* **1990**, *11*, 619−624.
(28) Saltzman, W. M.; Radomsky, M. L.; Whaley, K. J.; Cone, R. A. *Biophys. J.* **1994**, *66*, 508−515.
(29) Grathwohl, P. *Diffusion in Natural Porous Media: Contaminant Transport, Sorption/Desorption and Dissolution Kinetics*; Kluwer Academic Publishers: New York, 1998.
(30) Fritzsche, C. *Appl. Environ. Microbiol.* **1994**, *60*, 1687−1689.
(31) Hao, O. J.; Richard, M. G.; Jenkins, D.; Blanch, H. W. *Biotechnol. Bioeng.* **1983**, *25*, 403−416.
(32) Longmuir, I. S. *Biochem. J.* **1954**, *57*, 81−87.
(33) Johnson, M. J. *J. Bacteriol.* **1967**, *94*, 101−108.
(34) Shaler, T. A.; Klecka, G. M. *Appl. Environ. Microbiol.* **1986**, *51*, 950−955.
(35) Chen, J.; Tannahill, A. L.; Shuler, M. L. *Biotechnol. Bioeng.* **1985**, *27*, 151−155.
(36) Blanch, H. W.; Clark, D. S. *Biochemical Engineering*; Marcel Dekker: New York, 1996.
(37) Pirt, S. J. *Principles of Microbe and Cell Cultivation*; Blackwell Scientific: Oxford, 1975.
(38) Logan, B. E.; Zhang, H. S.; Mulvaney, P.; Milner, M. G.; Head, I. M.; Unz, R. F. *Appl. Environ. Microbiol.* **2001**, *67*, 2499−2506.
(39) Maier, R. M.; Pepper, I. L.; Gerba, C. P. *Environmental Microbiology*; Academic Press: New York, 2000.
(40) Corapcioglu, M. Y.; Fedirchuk, P. *J. Contam. Hydrol.* **1999**, *36*, 209−230.
(41) Corapcioglu, M. Y.; Chowdhury, S.; Roosevelt, S. E. *Water Resour. Res.* **1997**, *33*, 2547−2558.
(42) Robbins, G. A. *Water Resour. Res.* **1989**, *25*, 1249−1258.
(43) Sternberg, S. P. K.; Cushman, J. H.; Greenkorn, R. A. *Transp. Porous Media* **1996**, *23*, 135−151.
(44) Crane, F. E.; Gardner, G. H. F. *J. Chem. Engin. Data* **1961**, *6*, 283−287.
(45) Harleman, D. R. F.; Rumer, R. R. *J. Fluid Mech.* **1963**, 385−394.

Received for review July 4, 2002. Revised manuscript received December 30, 2002. Accepted January 27, 2003.

ES020128B